Figure S1. Analysis of the binding of TR compounds to ClpP using SPR, Related to Figure 2.

(A) Raw SPR binding curves for each TR compound at varied concentrations.

(B) Fits of SPR data in A to the 1:1 Langmuir binding model. The obtained K_ds are given in each panel together with the respective errors from the fit.

Figure S1

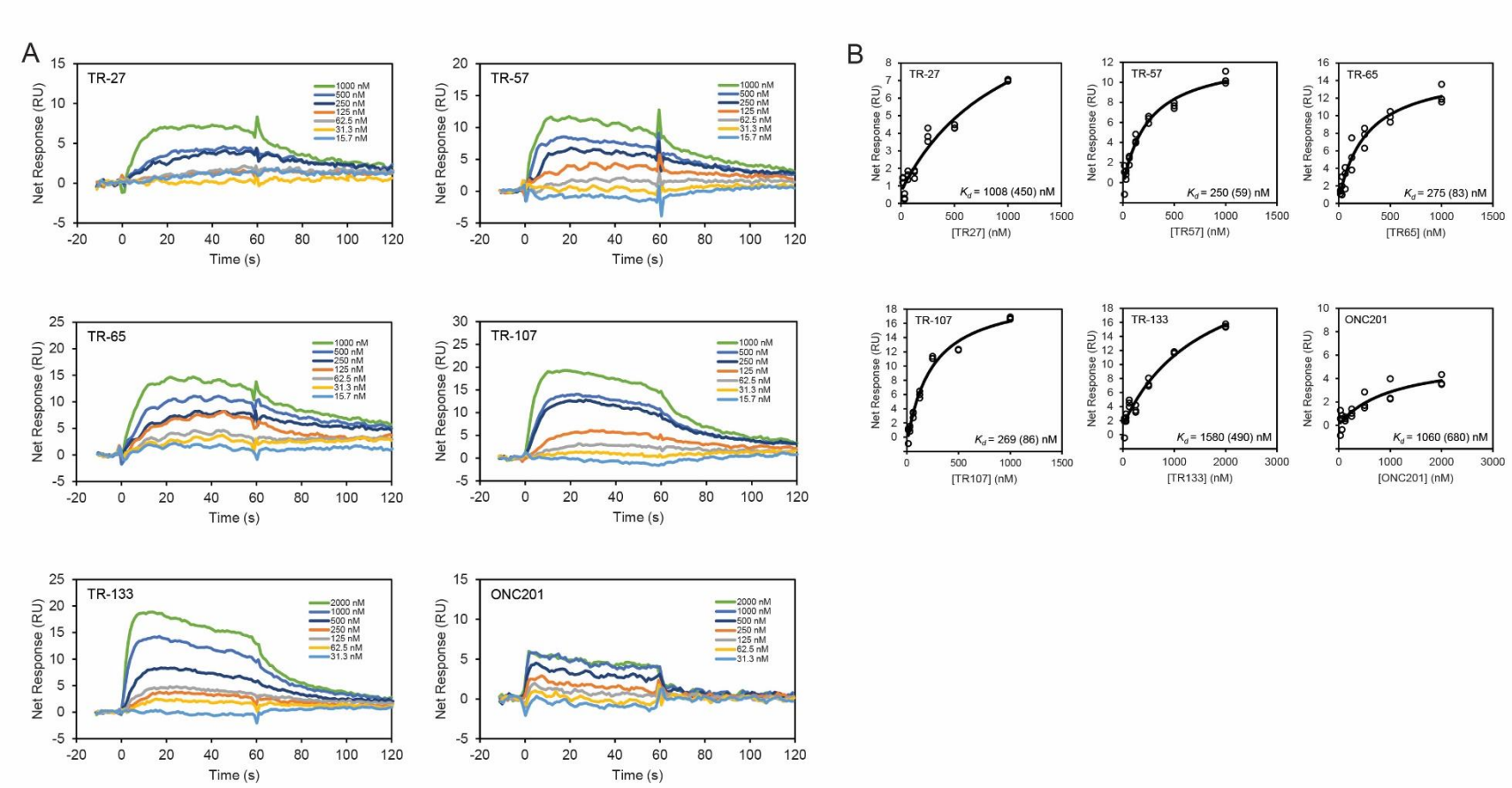
A
TR-27
TR-57
TR-65
TR-107
TR-133
ONC201
Net Response (RU)
Time (s)
1000 nM
500 nM
250 nM
125 nM
62.5 nM
31.3 nM
15.7 nM
2000 nM
B
TR-27
TR-57
TR-65
TR-107
TR-133
ONC201
K_d = 1008 (450) nM
K_d = 250 (59) nM
K_d = 275 (83) nM
K_d = 269 (86) nM
K_d = 1580 (490) nM
K_d = 1060 (680) nM
[TR27] (nM)
[TR57] (nM)
[TR65] (nM)
[TR107] (nM)
[TR133] (nM)
[ONC201] (nM)

Figure S2. The phenyl ring moieties of TR compounds exhibit shape and surface charge complementarity with the small pockets of H-sites, Related to Figure 4.

(A) On the left panel, shown is the TR-57 bound to the H-site, whose outer boundaries are covered with surface charges. On the right panel, the chemical structure of TR-57 is shown.

(B) Shown on the left panel is a cut-away view of the TR binding cavity showing the electrostatic potential of the two small cavities where the substituted phenyl ring moieties of TR-57 bind. Not only does TR-57 have a complementary shape with the small pockets, but the additional polar halide and nitrile groups enhance its affinity for the charged pockets. The right panel is in the same orientation as the left except that the molecular surface is transparent.

(C) The left panel shows the same binding cavity as in B but rotated by 180° around the y-axis to display the electrostatic potential map of the other side of the TR binding pocket. The right panel is a transparent representation of the molecular surface on the left panel.

Figure S2

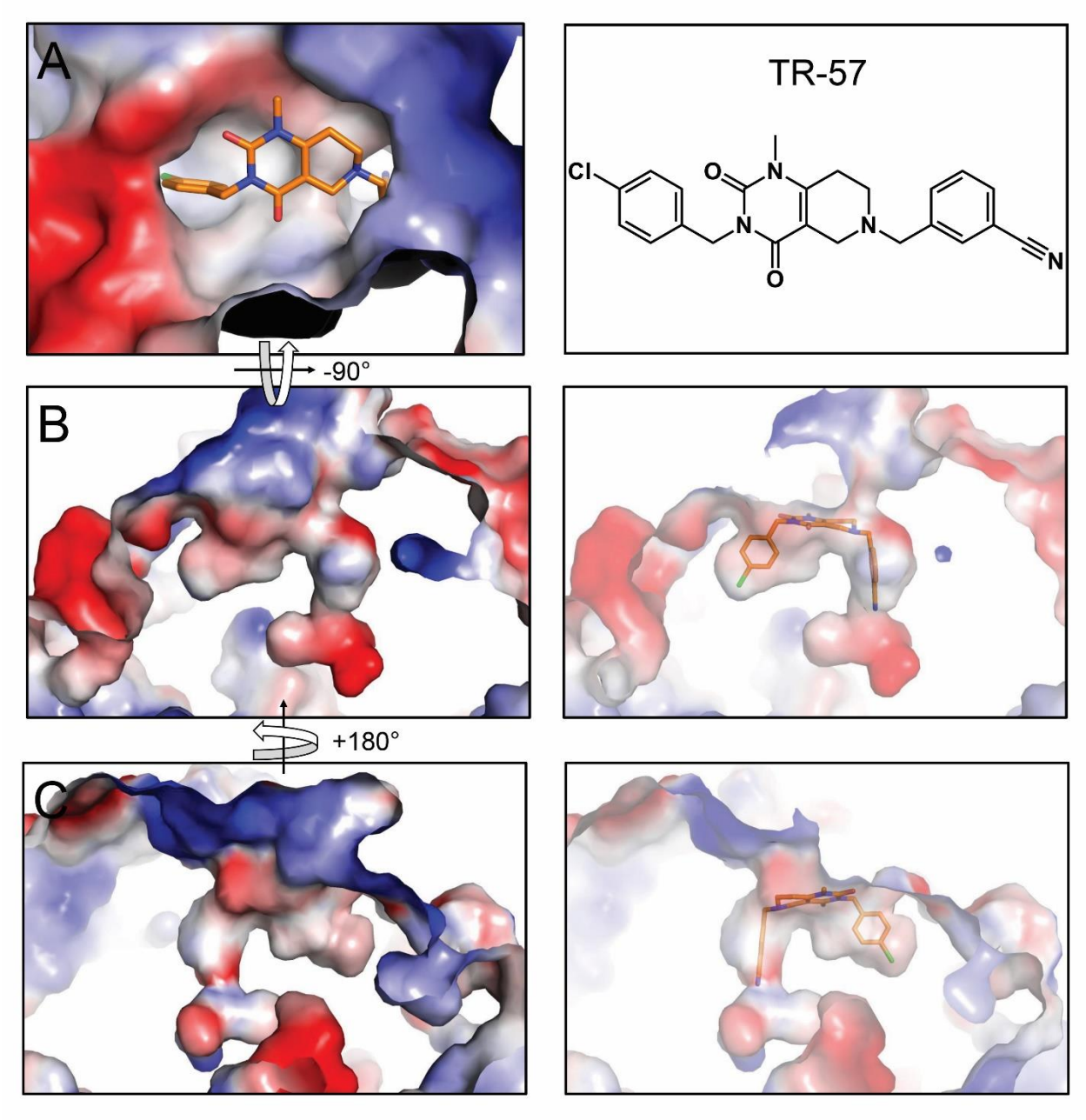

Figure S3. Confirming the absence of apoptosis in TR-27-treated cells by light/DAPI-fluorescence microscopy and western blotting, Related to Star Methods.

(A) Light (panels i, iv, vii and x) and DAPI-fluorescence (panels ii, v, viii and xi) microscopy and corresponding merged images (panels iii, vi, ix and xii) for MDA-MB-231 WT cells treated with 1 μM TR-27 (panels i to iii) or DMSO (panels iv to vi) and *CLPP*$^{-/-}$ cells treated with 1 μM TR-27 (panels vii to ix) or DMSO (x to xii). Drug / DMSO exposure was for 24 hours.

(B) Western blots for ClpP, ClpX, Mcl1, caspase 9, caspase 3, and caspase 8 on total cell lysates derived from MDA-MB-231 WT and *CLPP*$^{-/-}$ cells treated with 1 μM TR-27 or DMSO for 24 hours. GAPDH was used as a loading control. The "pro" in the anti-caspase blots refers to the full-length inactive forms of the three caspases prior to proteolytic cleavage during apoptotic onset.

(C) Western blots of caspase 9 from total cell lysates derived from MDA-MB-231 WT and *CLPP*$^{-/-}$ cells treated with either 1 μM TR-27 (vs. DMSO) for 24 hours or 2 μM doxorubicin (vs. DMSO) for 72 hours. GAPDH was used as a loading control. "pro" refers to the full-length inactive form of caspase 9 while p37 and p35 refer to the two fragments generated after its cleavage and activation.

Figure S3

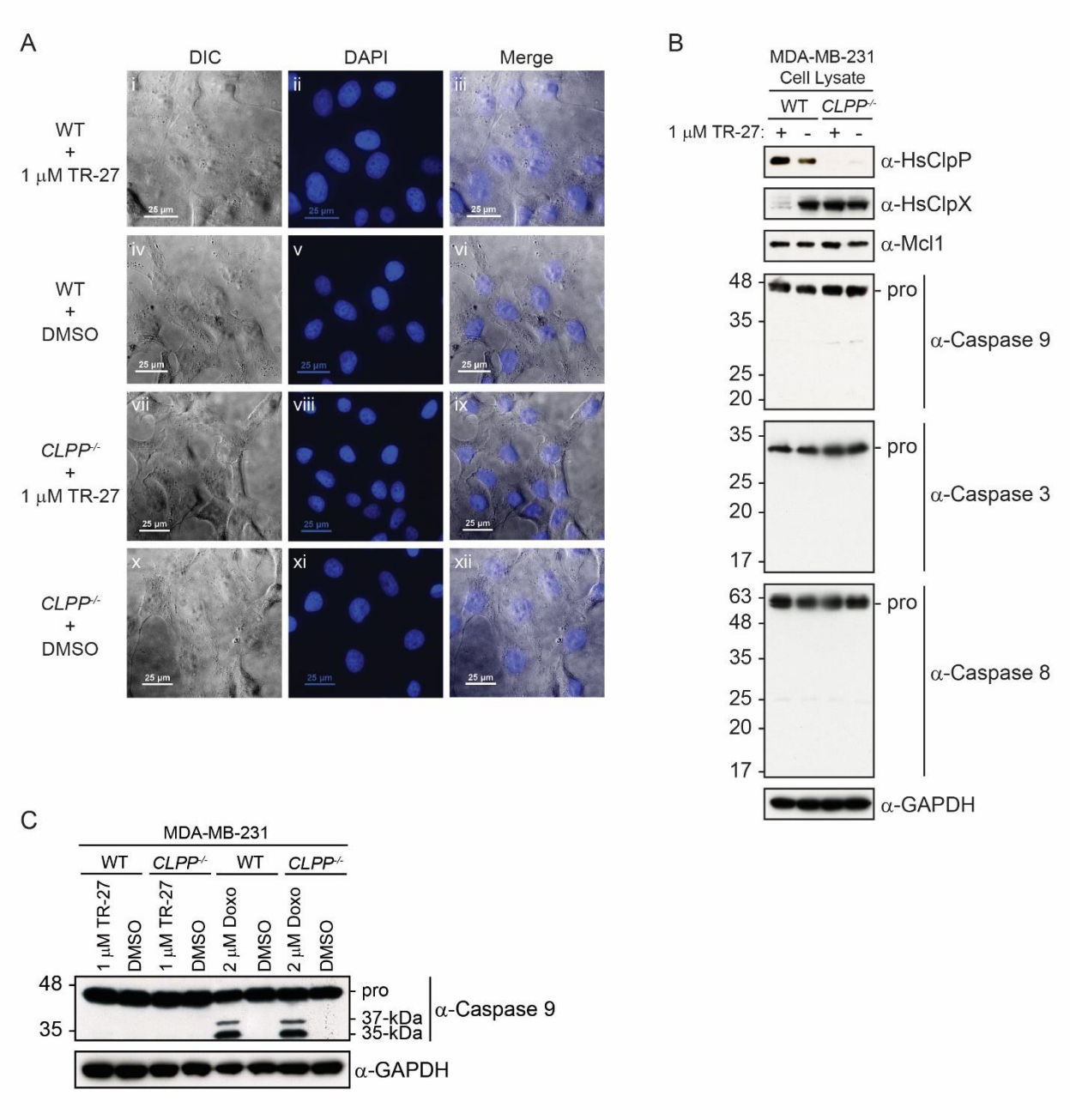
A
DIC
DAPI
Merge
WT + 1 μM TR-27
WT + DMSO
CLPP-/- + 1 μM TR-27
CLPP-/- + DMSO
25 μm
B
MDA-MB-231 Cell Lysate
WT
CLPP-/-
1 μM TR-27: + - + -
α-HsClpP
α-HsClpX
α-Mcl1
48
35
25
20
pro
α-Caspase 9
35
25
20
17
pro
α-Caspase 3
63
48
35
25
20
17
pro
α-Caspase 8
α-GAPDH
C
MDA-MB-231
WT
CLPP-/-
WT
CLPP-/-
1 μM TR-27
DMSO
1 μM TR-27
DMSO
2 μM Doxo
DMSO
2 μM Doxo
DMSO
48
35
pro
37-kDa
35-kDa
α-Caspase 9
α-GAPDH

Figure S4. Schematics of the experimental workflow and data analysis protocols used for the HYTANE experiments, Related to Star Methods.

(A) Cell culturing and sample preparation. When cells were harvested, they were washed with PBS to remove residual media. 3 replicates were prepared per cell line per condition.

(B) Sample processing for HYTANE. The N- and C-termini of a protein molecule are shown as "N" and "C", respectively. The N-terminal peptide to be isolated and analyzed is shown in purple; the rest of the protein and corresponding peptides generated after trypsin digestion (step 8) are shown in cyan. Yellow diamonds represent dimethylation of free amine groups (including the N-terminus). Red rods represent hydrophobic tags that facilitate the subsequent removal of the tagged peptides using C18 columns.

(C) Flow chart for the analysis of HYTANE data. Determination of whether an observed change in abundance of a given peptide was due to TR-27's effect or whether it was dependent on the presence of ClpP occurs where indicated with asterisks (*). The abundance data of both novel and native N-terminal peptides were subjected to further analysis.

(D) Scatter plots of $\log_2$ ratios of MDA-MB-231 *CLPP*$^{-/-}$ with TR-27 treatment to DMSO (no drug) treatment versus the corresponding $\log_2$ ratios for WT cells. Red data points correspond to N-terminal peptides that are deemed to show statistically significant changes in abundance in WT cells treated with TR-27 compared to DMSO with $p < 0.05$ based on comparison of $\log_2$ [(WT + TR-27)/(WT + DMSO)] versus $\log_2$ [(*CLPP*$^{-/-}$ + TR-27)/(*CLPP*$^{-/-}$ + DMSO)] for each N-terminal peptide. Green data points correspond to those that are deemed to display insignificant changes with $p \geq 0.05$. Panels: (i) $p < 0.05$ (red) data points and $p \geq 0.05$ (green) data points shown together; (ii) $p \geq 0.05$ data points only; (iii) $p < 0.05$ data points only. Dotted line defines the trend expected when TR-27 treatment induces equal changes in peptide abundance in both WT and *CLPP*$^{-/-}$.

Figure S4

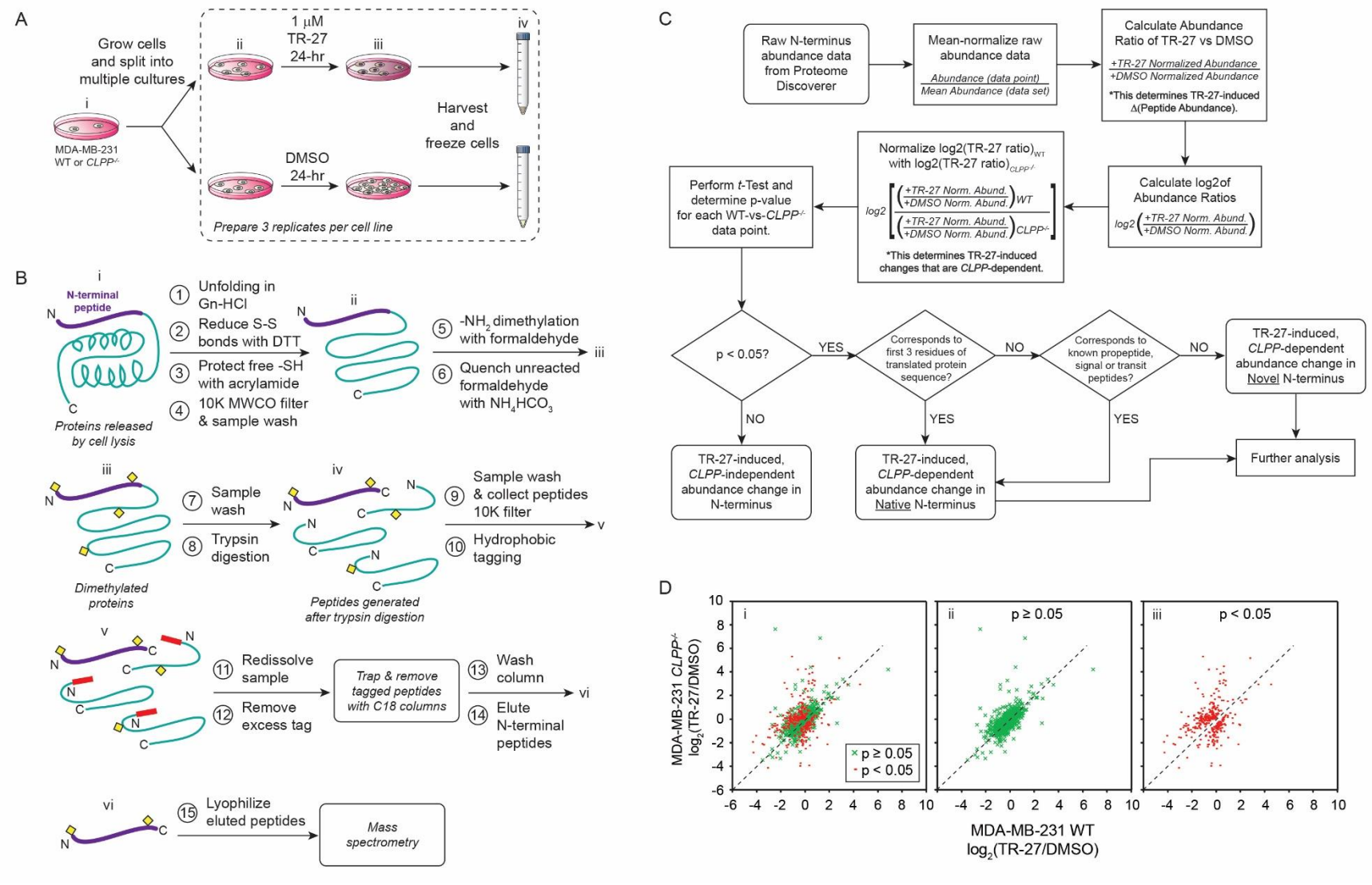
A
Grow cells and split into multiple cultures
MDA-MB-231 WT or CLPP-/-
1 μM TR-27 24-hr
DMSO 24-hr
Harvest and freeze cells
Prepare 3 replicates per cell line
B
N-terminal peptide
Proteins released by cell lysis
1 Unfolding in Gn-HCl
2 Reduce S-S bonds with DTT
3 Protect free -SH with acrylamide
4 10K MWCO filter & sample wash
5 -NH2 dimethylation with formaldehyde
6 Quench unreacted formaldehyde with NH4HCO3
Dimethylated proteins
7 Sample wash
8 Trypsin digestion
Peptides generated after trypsin digestion
9 Sample wash & collect peptides 10K filter
10 Hydrophobic tagging
11 Redissolve sample
12 Remove excess tag
Trap & remove tagged peptides with C18 columns
13 Wash column
14 Elute N-terminal peptides
15 Lyophilize eluted peptides
Mass spectrometry
C
Raw N-terminus abundance data from Proteome Discoverer
Mean-normalize raw abundance data
Abundance (data point) / Mean Abundance (data set)
Calculate Abundance Ratio of TR-27 vs DMSO
+TR-27 Normalized Abundance / +DMSO Normalized Abundance
*This determines TR-27-induced Δ(Peptide Abundance).
Calculate log2of Abundance Ratios
Normalize log2(TR-27 ratio)WT with log2(TR-27 ratio)CLPP-/-
*This determines TR-27-induced changes that are CLPP-dependent.
Perform t-Test and determine p-value for each WT-vs-CLPP-/- data point.
p < 0.05?
YES
NO
Corresponds to first 3 residues of translated protein sequence?
Corresponds to known propeptide, signal or transit peptides?
TR-27-induced, CLPP-independent abundance change in N-terminus
TR-27-induced, CLPP-dependent abundance change in Native N-terminus
TR-27-induced, CLPP-dependent abundance change in Novel N-terminus
Further analysis
D
MDA-MB-231 CLPP-/- log2(TR-27/DMSO)
MDA-MB-231 WT log2(TR-27/DMSO)
p ≥ 0.05
p < 0.05

Figure S5. TFAM and Grp75 are targeted for degradation by TR-27-activated ClpP, Related to Figures 5 and 6.

(A) Shown are western blots analyzing the expression of TFAM and Grp75 in MDA-MB-231 WT and *CLPP*$^{-/-}$cells treated with 1 μM TR-27, 6 μM ADEP-14, or DMSO for 24 hours. GAPDH serves as the sample loading control.

(B) Degradation of TFAM in the presence of ClpP and TR-65. Samples were collected every hour for 5 hours. Two negative controls were performed: ClpP only and TR-65 only. The blue arrow points to ClpP. The red arrow points to TFAM. Note that although TFAM has a higher MW than ClpP, it runs lower on the gel. This could be because it has a greater percent composition of arginine and lysine; as a result, TFAM would bind more SDS and traverse through the gel at a faster rate.

(C) The two bands at about 15 kDa and 9 kDa are TFAM degradation fragments generated by activated ClpP, which were subjected to N-terminal sequencing. High concentrations of ClpP and TFAM were used to achieve an abundance of degraded bands visible by eye on a Coomassie stained gel, as such the bands at about 25 kDa are composed of both TFAM and ClpP.

(D) Shown is a cartoon representation of the domains of TFAM. The two red arrows point to the two cut sites caused by activated ClpP identified by N-terminal sequencing of the bands indicated in C.

(E) Shown are the cut site in TFAM mapped onto the protein structure (PDB id 3TQ6)[1]. The structure was generated using PyMOL.

Figure S5

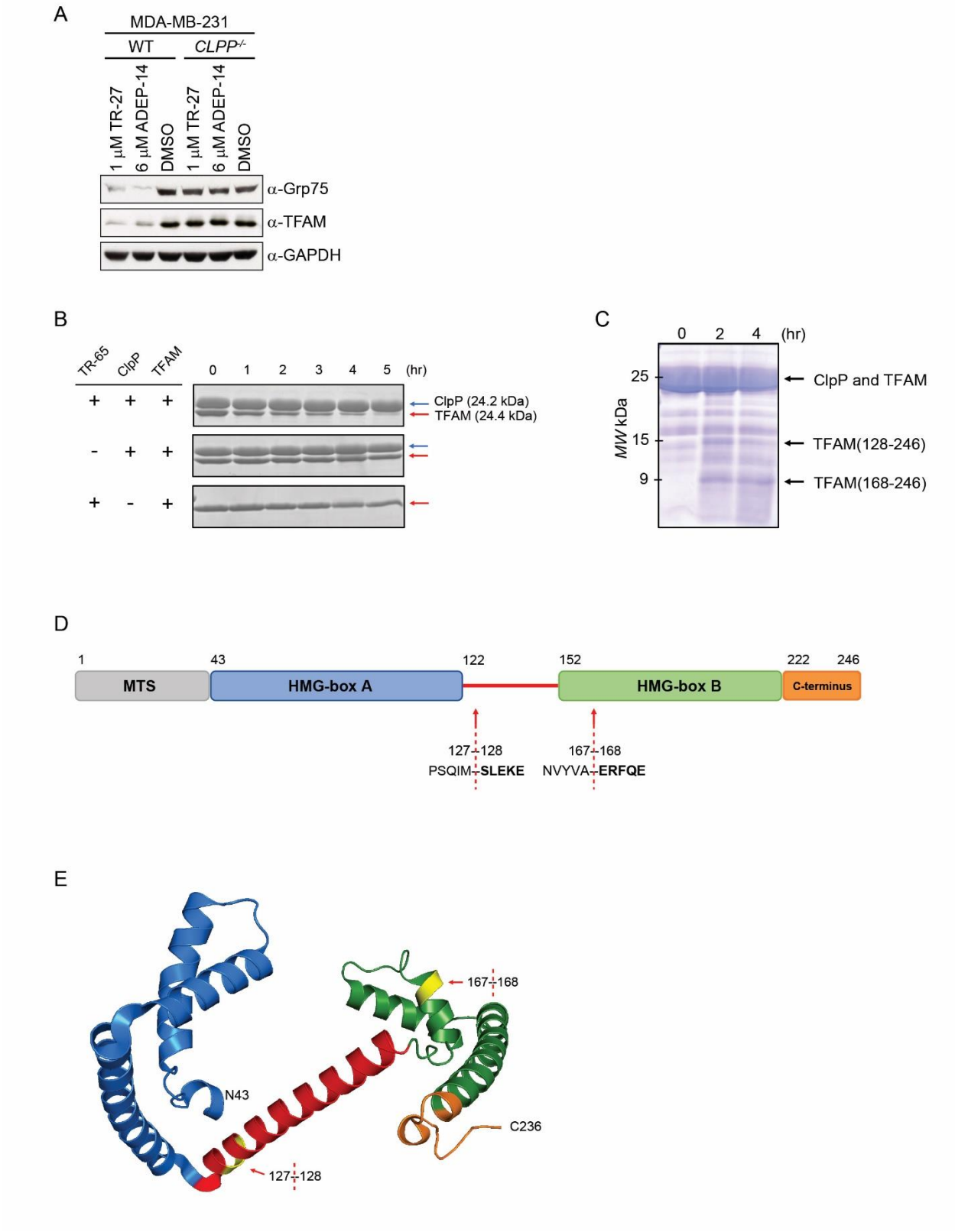
A
MDA-MB-231
WT
CLPP-/-
1 μM TR-27
6 μM ADEP-14
DMSO
1 μM TR-27
6 μM ADEP-14
DMSO
α-Grp75
α-TFAM
α-GAPDH
B
TR-65
ClpP
TFAM
0 1 2 3 4 5 (hr)
ClpP (24.2 kDa)
TFAM (24.4 kDa)
C
0 2 4 (hr)
MW kDa
25
15
9
ClpP and TFAM
TFAM(128-246)
TFAM(168-246)
D
1
43
122
152
222
246
MTS
HMG-box A
HMG-box B
C-terminus
127-128
PSQIM-SLEKE
167-168
NVYVA-ERFQE
E
167-168
N43
C236
127-128

Figure S6. Synthesis of TR-27 and TR-65, Related to Star Methods.

Shown is a schematic for the synthesis of TR-27 and TR-65 compounds. (a) NaBH(OAc)3, CH2Cl2, 30oC/4 h, (b) MeI, MeOH, reflux/30 min, (c) dioxane, reflux/12h, and (d) MeONa MeOH, reflux/12 h.

Figure S6

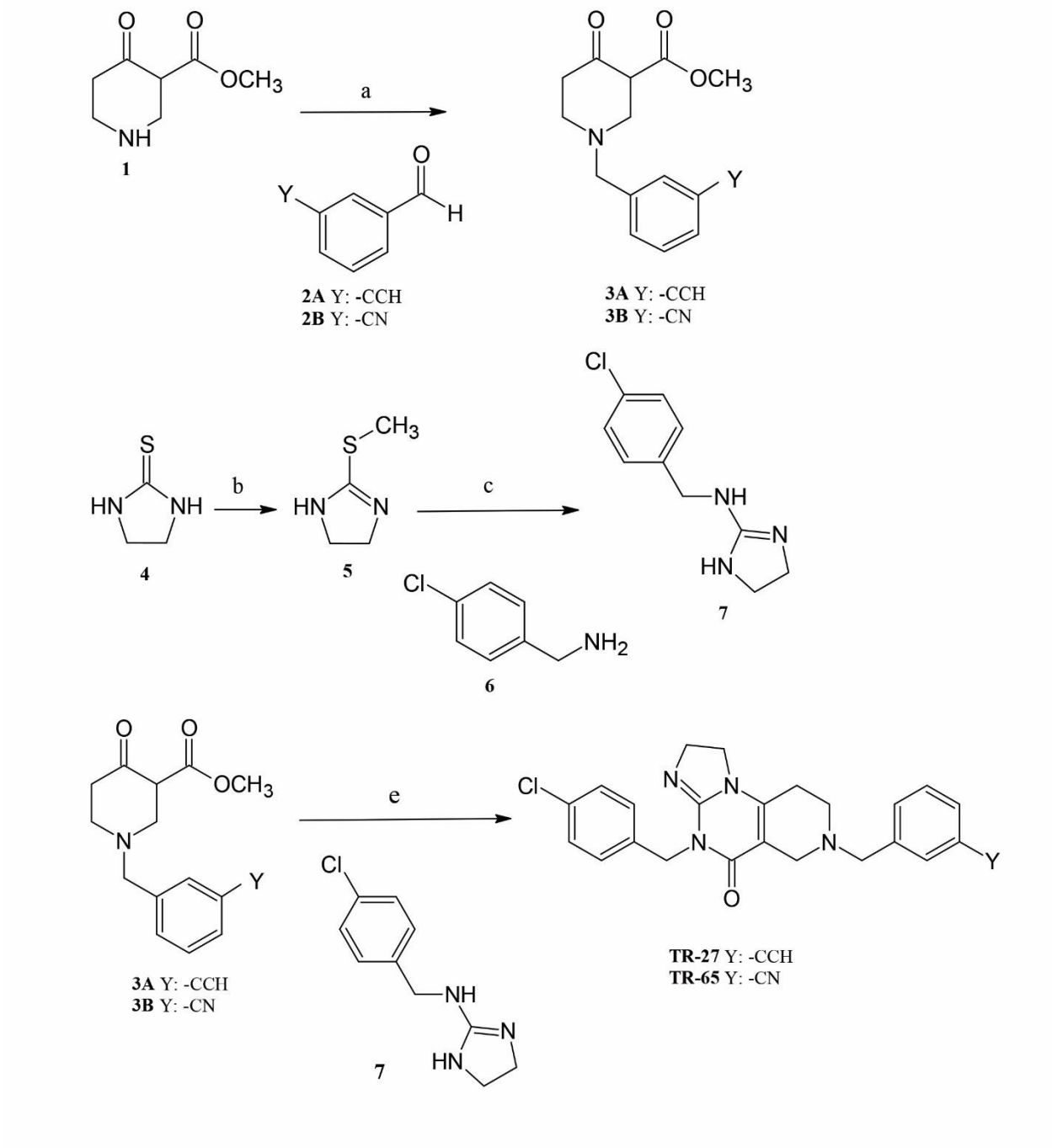

Figure S7. Synthesis of TR-57, TR-107, and TR-133, Related to Star Methods.

(A) Shown is a schematic for the synthesis of TR-57. (a) aq NH_3, EtOH, Na_2CO_3, 70^oC/4 h; (b) Et3N, toluene, 80^oC/8 h and (c) MeI, DMF, 100^oC/12 h.

(B) Shown is a schematic for the synthesis of TR-107 and TR-133. (a) CH_4N_2, HOAc, reflux/8 h and (b) Cs_2CO_3, (TR-107: pClBnBr, TR-133: pBrBnBr), THF, reflux/12 h.

Figure S7

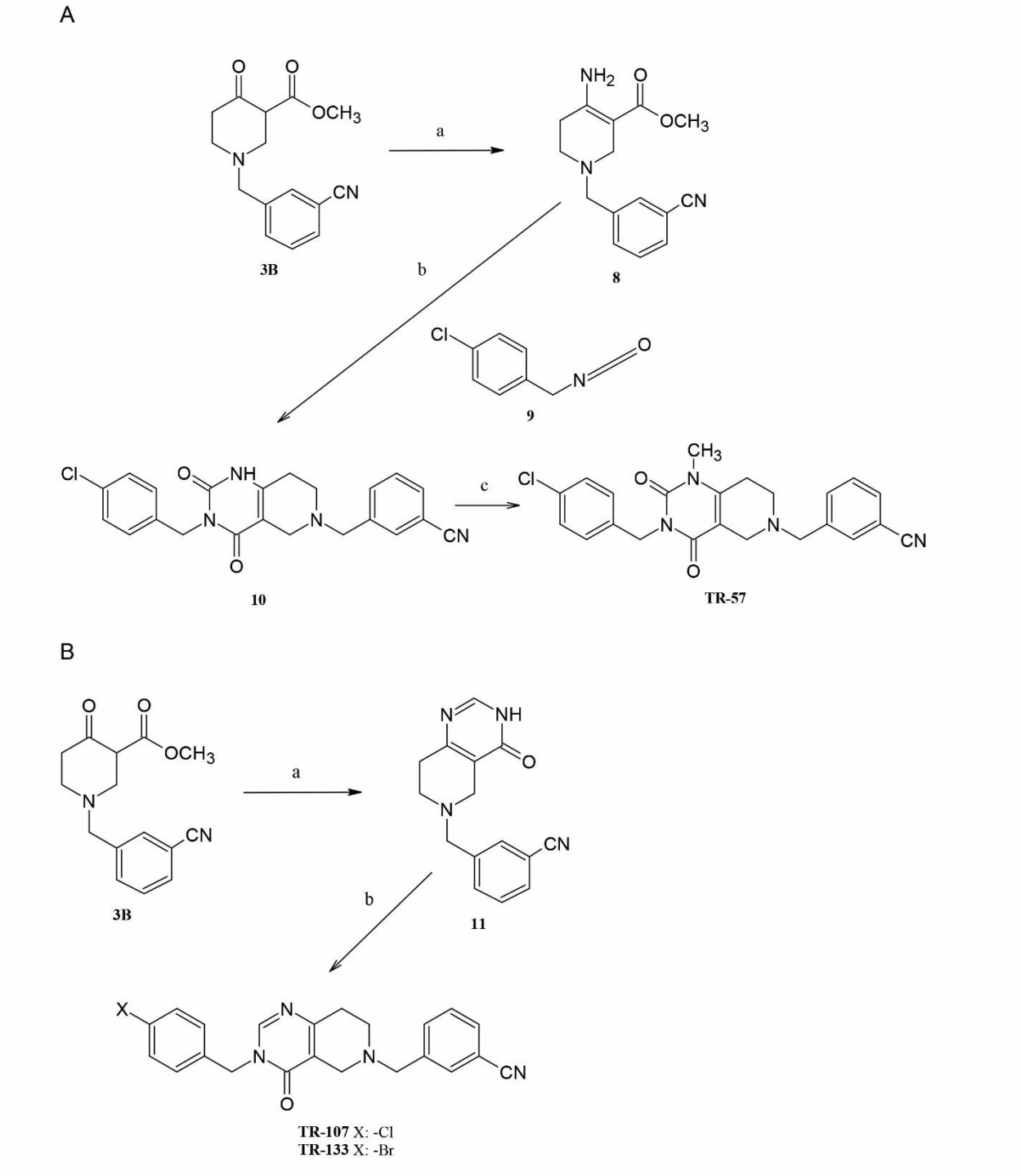

LEGENDS FOR SUPPLEMENTAL TABLES

Table S1. X-ray data collection and refinement statistics for complexes of human ClpP with TR compounds, Related to Figure 3.

Table S2. Buried surface area for different small molecule activators upon complex formation with human ClpP, Related to Figure 4.

Table S3. Proteins and protein complexes detected in both HYTANE and BioID, Related to Figure 5.

Table S1

Table S1. X-ray data collection and refinement statistics for complexes of human ClpP with TR compounds, Related to Figure 3.

TR compound **PDB ID**	**TR-27** **7UVM**	**TR-57** **7UVN**	**TR-65** **7UVR**	**TR-107** **7UVU**	**TR-133** **7UW0**
Data collection					
Space group	C 1 2 1	C 1 2 1	C 1 2 1	C 1 2 1	I 1 2 1
Cell dimensions *a*, *b*, *c* (Å) *α*, *β*, *γ* (°)	 143.15, 153.72, 105.10 90.00, 117.76, 90.00	 142.10, 153.04, 104.70 90.00, 117.92, 90.00	 142.17, 152.52, 104.27 90.00, 118.10, 90.00	 142.15, 152.66, 104.34 90.00, 118.00, 90.00	 105.66, 153.80, 133.21 90.00, 107.03, 90.00
Resolution (Å)	29.62 - 2.19 (2.25 - 2.19)	50.00 – 3.10 (3.15 – 3.10)	29.35 - 2.86 (2.93 - 2.86)	50.00 - 3.30 (3.36 - 3.30)	93.62 - 2.80 (2.89 - 2.80)
I/σI	5.2/1.3	11.4/1.8	6.0/1.4	4.7/1.2	4.2/1.7
Rmerge	0.235 (0.737)	0.285 (1.065)	0.207 (0.837)	0.205 (0.879)	0.354 (0.963)
CC 1/2	0.987 (0.716)	0.992 (0.705)	0.987 (0.628)	0.964 (0.570)	0.805 (0.420)
Completeness (%)	99.2 (90.2)	99.7 (99.4)	99.2 (91.9)	98.7 (96.6)	95.2 (94.3)
Redundancy	7.0 (5.9)	7.2 (7.3)	5.2 (4.8)	6.6 (6.1)	4.9 (4.9)
Refinement					
Resolution (Å)	29.40 - 2.19	50.00 – 3.10	29.17 – 2.86	46.06 – 3.30	50.51 - 2.80
No. reflections	102,283 (9,495)	35,028 (3,309)	44,927 (4,367)	29,842 (2,427)	47,166 (4,706)
R_{work}/R_{free}	0.1971/0.2370	0.2291/0.2823	0.2028/0.2526	0.1900/0.2599	0.2606/0.3080
No. of atoms Macromolecules Ligands Solvent	 9,616 378 428	 9,809 210 238	 9,547 217 110	 9,763 196 125	 9,963 196 70
B-factors (Å^2) Protein Ligands Water	 43.30 42.76 46.60	 51.55 49.87 48.71	 47.02 45.34 41.28	 49.37 48.32 38.96	 23.77 24.08 12.56
r. m. s. d. Bond lengths (Å) Bond angles (°)	 0.015 1.470	 0.002 0.60	 0.012 1.35	 0.012 1.390	 0.002 0.56
Ramachandran Favored Allowed Disallowed	 97.07 2.68 0.25	 95.65 3.86 0.49	 95.26 4.32 0.42	 91.36 7.57 0.00	 96.26 3.49 0.25

Statistics for the highest-resolution shell are shown in parentheses.

Table S2

Table S2. Buried surface area for different small molecule activators upon complex formation with human ClpP, Related to Figure 4.

Small molecule	Surface area ($Å^2$)	Buried surface area upon binding ($Å^2$)	Percent buried (%)
TR-27	665	564	84.8
TR-57	642	530	82.6
TR-65	650	534	82.2
TR-107	610	511	83.8
TR-133	619	522	84.3
ONC201	607	495	81.5
ADEP-28	951	707	74.3
ZG111	758	639	84.3
D9*	596**	516	86.6

*Y118A mutant of human ClpP was used in crystallization with small molecule.
**Considering major pose of small molecule in coordinate file PDB id 6H23.

Table S3

TABLE S3. Proteins and protein complexes detected in both HYTANE and BioID, Related to Figure 5.

Protein / Protein Complex	Functional Category	Protein / Protein Subunit	HYTANE (Native or Novel)	BioID[1]
NADH:ubiquinone dehydrogenase (Complex I)	Energy metabolism (OXPHOS)	NDUFA2		↓
		NDUFA6		↓
		NDUFA7		↓
		NDUFA12	Native↓	↓
		NDUFB4	Native↓	
		NDUFB8	Native↓	
		NDUFS2*	Native↓	↓
		NDUFS4		↓
		NDUFS6		↓
		NDUFS7		↓
		NDUFS8	Native↓	↓
		NDUFV2	Novel ↓	↓
		NDUFV3		↓
Succinate dehydrogenase (Complex II)	Energy metabolism (OXPHOS)	SDHA		↓
		SDHB	Native↓	↓
Ubiquinol-cytochrome c oxidoreductase (Complex III)	Energy metabolism (OXPHOS)	UQCRB	Native↓	↓
		UQCRC1	Native↓	
Cytochrome c oxidase (complex IV)	Energy metabolism (OXPHOS)	COX4I1	Native↓	↓
		COX5A		↓
		COX5B	Native↓	↓
		COX6C	Native↓	
2-Oxoglytarate dehydrogenase complex	Energy metabolism (TCA cycle)	OGDH		↓
		DLST	Native↓	
GTP-specific succinyl-CoA synthase complex	Energy metabolism (TCA cycle)	SUCLG1		↓
		SUCLG2	Native↓	↓
Malate dehydrogenase	Energy metabolism (TCA cycle)	MDH2	Native↓	↓
Isocitrate dehydrogenase	Energy metabolism (TCA cycle)	IDH3A		↓
		IDH3G	Native↓	
Complex I α-subcomplex assembly factor 2	Molecular chaperone	NDUFAF2	Native↓	↓
Complex I α-subcomplex assembly factor 3	Molecular chaperone	NDUFAF3	Novel ↓	↓
		NDUFS2*	Native↓	↓
Mitochondrial ribosome 39S (large) subunit	Mitochondrial translation	MRPL4	Novel ↓	
		MRPL10		↓
		MRPL12		↓
		MRPL14		↓
		MRPL19		↓
		MRPL21		↓
		MRPL40		↓

		MRPL42	Novel ↓	
		MRPL44		↓
		MRPL45		↓
		MRPL46	Novel ↓	↓
		MRPL47		↓
		MRPL48		↓
		MRPL49	Novel ↓	
		MRPL54		↓
		MRPL55		↓
Mitochondrial ribosome 28S (small) subunit	Mitochondrial translation	MRPS2	Novel ↓	
		MRPS6		↓
		MRPS7		↓
		MRPS11		↓
		MRPS15		↓
		MRPS16		↓
		MRPS17		↓
		MRPS18A	Novel ↓	
		MRPS23		↓
		MRPS24		↓
		MRPS25		↓
		MRPS26		↓
		MRPS27	Native ↓	
		MRPS28	Native ↓	↓
		MRPS29	Novel ↓	
		MRPS35	Novel ↓	
		MRPS36	Novel ↓	↓
Mitochondrial elongation factor G	Mitochondrial translation	GFM1	Native ↓	↓
Mitochondrial transcription factor A	Mitochondrial transcription	TFAM	Native ↓	↓
Glutamate dehydrogenase 1	Amino acid metabolism	GLUD1	Native ↓	↓
Hydroxyacyl-CoA dehydrogenase	Lipid metabolism (β-oxidation)	HADH	Native ↓	↓
Enoyl-CoA hydratase 1	Lipid metabolism (β-oxidation)	ECHS1	Native ↓	↓
Acetyl-CoA acetyltransferase 1	Lipid metabolism (β-oxidation)	ACAT1	Native ↓	↓
Adenosine 5'-monophosphoramidase	Nucleic acid metabolism (purine)	HINT2	Novel ↓	↓
*NDUFS2 is found in complex with both NADH:ubiquinone dehydrogenase (Complex I) and Complex I α-subcomplex assembly factor 3.				

[1]The BioID data are derived from Ishizawa et al. (2019) *Cancer Cell* 35, 721-737, e729.

REFERENCES

1. Rubio-Cosials, A., Sydow, J.F., Jiménez-Menéndez, N., Fernández-Millán, P., Montoya, J., Jacobs, H.T., Coll, M., Bernadó, P., and Solà, M. (2011). Human mitochondrial transcription factor A induces a U-turn structure in the light strand promoter. Nature Structural & Molecular Biology *18*, 1281-1289. 10.1038/nsmb.2160.